Torque Ripple Reduction of SRM Drive Using Improved Direct Torque Control with Sliding Mode Controller and Observer

Xiaodong Sun, *Senior Member, IEEE*, Jiangling Wu, Gang Lei, *Member, IEEE*, Youguang Guo, *Senior Member, IEEE*, and Jianguo Zhu, *Senior Member, IEEE*

***Abstract*—The industrial application of the switched reluctance motor (SRM) is limited by its high torque ripples caused by the doubly salient structure. In this paper, an improved direct torque control (DTC) with sliding mode controller and observer is developed to reduce the torque ripples of a four-phase SRM. Firstly, a sliding mode controller based on a new reaching law is developed for designing a sliding mode speed controller (SMSC) for the DTC system. An anti-disturbance sliding mode observer (ADSMO) is then proposed and combined with the SMSC to build a composite anti-disturbance speed control strategy. Moreover, detailed simulation validations are carried out to reveal the effectiveness of the new reaching law, SMSC and ADSMO. Finally, experiments are conducted to verify the performance of the proposed SMSC-ADSMO in a DTC system with a four-phase SRM prototype.**

***Index terms*- Torque ripple reduction, direct torque control, switched reluctance motor, sliding mode speed controller, anti-disturbance sliding mode observer**

I. INTRODUCTION

The switched reluctance motor (SRM) has been utilized widely in many industrial devices and systems owing to its simple and robust structure, low cost, high fault tolerance, high torque density, and high efficiency in a wide speed range [1]. However, it suffers from the high torque ripples due to its inherent doubly salient structure, which makes it inferior to the permanent magnet synchronous motor (PMSM) in some high-performance applications, like electric vehicles [2]-[4]. To overcome this drawback, advanced torque control strategies have been developed and reported in many research works [5]-[7]. There are mainly three methods, torque sharing function (TSF) method, direct instantaneous torque control (DITC) and direct torque control (DTC).

In [5], an offline TSF was introduced for torque ripple reduction in SRM. The TSF uses static flux linkage characteristics of the motor to determine optimal current profiles to reduce torque ripple by achieving minimal copper losses. However, as the speed increases, the back electromotive force (EMF) of the motor continues to increase, and the tracking performance of the current or flux controller weakens, which makes the motor torque unable to follow the reference torque effectively.

In [6], a DITC based on a fractional-order proportional integral differential (PID) controller was proposed to reduce the torque ripple and improve the dynamic performance. It does not need accurate rotor position. However, its constant torque speed range is limited by the motor back EMF.

As a torque control method, DTC was firstly used in AC motors. Compared with TSF and DITC, it has the merits of simple structure, fast torque response, wide speed adaptation range, and good robustness. Thus, it is becoming popular in the control of SRM drive systems [7]. However, the bang-bang control algorithm of the conventional DTC based on the torque and flux linkage hysteresis control of single voltage vector inevitably results in unsteady switching frequency and large flux and torque ripples [8]. To overcome these drawbacks, various works have been reported in the literature.

In [9], to improve the net torque per ampere ratio of the DTC strategy, a new DTC strategy by modifying the partition of the sectors and appropriate voltage vector selection was proposed. A Lyapunov function-based DTC was presented in [10] for the minimization of torque ripples in an SRM drive system by tracking the phase torque references accurately. In [11], a unified controller including DTC for SRMs was proposed for wide speed operations. The proposed controller can minimize the output torque ripples at low and medium speeds and operate in a single pulse mode at high speed. An improved DTC method was reported in [12] to reduce the torque ripples by reorganizing the sectors and tracking the torque reference accurately.

These studies mainly concentrated on tracking the phase of torque references via utilizing an improved partition of the sectors or combining with other control strategies to determine the sharing function of torque during commutations. None of them focused on improving the torque control by enhancing speed control and anti-interference ability of DTC in real-time.

As a variable structure control, sliding mode control (SMC) can continuously and purposefully change according to the current state of the system during the dynamic process, forcing the system to move according to the predetermined sliding mode state trajectory. The sliding mode can be designed and has nothing to do with the object parameters and disturbances, which makes the SMC have the advantages of fast response, corresponding parameter changes and disturbance insensitivity

Manuscript received March 10, 2020; revised April 21, 2020, May 27, 2020, and June 24, 2020; accepted August 11, 2020. This work was supported by the National Natural Science Foundation of China under Project 51875261, the Natural Science Foundation of Jiangsu Province of China under Projects BK20180046 and BK20170071, and the "Qinglan project" of Jiangsu Province. (*Corresponding author: Gang Lei*.)

X. Sun and J. Wu are with the Automotive Engineering Research Institute, Jiangsu University, Zhenjiang 212013, China (email: xdsun@ujs.edu.cn, jlwu_ujs@163.com).

G. Lei and Y. Guo are with the School of Electrical and Data Engineering, University of Technology Sydney, NSW 2007, Australia (e-mail: Gang.Lei@uts.edu.au, Youguang.Guo-1@uts.edu.au).

J. Zhu is with the School of Electrical and Information Engineering, University of Sydney, NSW, 2006, Australia (e-mail: jianguo.zhu@sydney.edu.au).

[13], [14]. Therefore, it is highly worthwhile to utilize the advanced SMC to substitute the conventional proportional-integral (PI) control and add an anti-interference module to enhance the stability of speed and torque, and then improve the torque control.

Advancement in SMC techniques has been widely studied in various industrial control systems [15]-[18]. For example, in [15], a new continuous terminal SMC algorithm was proposed to guarantee that the system states reach the sliding surface in finite time. Not only the robustness is guaranteed by the proposed controller but also the continuity makes the control algorithm more suitable for the servo mechanical systems. In [16], a robust tracking output-control strategy was proposed for a quadrotor under the influence of external disturbances and uncertainties. It is composed of a finite-time sliding-mode observer, a combination of PID controllers and continuous sliding mode controllers.

However, the application of SMC in SRM control is relatively rare. In [19] and [20], the SMC was used in current and flux linkage controllers, respectively. In [21] and [22], the SMC was designed as an observer to realize sensorless control of SRM.

Since the reaching law has a significant impact on the dynamic quality of the sliding mode approaching motion stage and the sliding mode chattering suppression effect, various advanced reaching laws have been investigated [23]-[25]. For example, in [23], a new nonlinear reaching law containing an exponential term was presented to design a sliding mode controller to settle the reaching time/chattering dilemma in the conventional SMC approach.

The sliding mode observer (SMO) is a type of dynamic system estimating the state variables based on the actual measurements of a system external variables. It uses nonlinear high gain feedback to force the estimated state to approach the hyperplane, making the estimated output equal the measured output [26]-[30]. For example, in [26], an extended sliding mode mechanical parameter observer was presented to track system disturbances in real-time, and a simple algorithm was developed for mechanical parameter estimation of a PMSM control system. In [27], an SMO was presented to obtain an accurate flux estimate without knowing the accurate input speed of the induction machine.

In this paper, the SMC and SMO are applied to the speed loop to improve the DTC system performance, such as obtaining the reference torque accurately, further realizing accurate control, reducing torque ripple, and improving the dynamic performance of the SRM. The main contributions of this paper are listed as follows:

1) To deal with the contradiction between the sliding mode reaching speed and chattering, a new reaching law (NRL) is proposed. It adds the system state variable and substitutes the symbolic function for hyperbolic tangent saturation function.
2) A sliding mode speed controller (SMSC) based on the NRL is designed.
3) An anti-disturbance sliding mode observer (ADSMO) is presented and combined with SMSC to build up an anti-disturbance composite speed control strategy. The principle of torque ripple reduction of the proposed control scheme is analyzed.

The remainder of this paper is organized as follows. Section II introduces the proposed SMC with an NRL. Section III presents the design of SMSC based on NRL in the DTC system. Section IV describes the design of ADSMO and a composite speed control strategy. Detail simulation validations in terms of NRL, SMSC and ADSMO are presented in Section V. Experimental validation is presented in Section VI, followed by the conclusions.

II. A New Reaching Law for the SMC

In order to improve the dynamic quality of the sliding mode approaching motion stage and the sliding mode chattering suppression effect, the conventional exponential reaching law (CERL) is used for control. It can be expressed as

$$\frac{ds}{dt} = -\eta \,\mathrm{sgn}(s) - ks, \quad \eta > 0, k > 0 \tag{1}$$

where ηsgn(s) is an isokinetic reach term, and ks an exponential reaching term. However, the CERL still suffers from the dilemma to increase the reaching speed and reduce the sliding chattering since its reaching speed is determined by the parameter k. Thus, a new reaching law is proposed by adding the variable coefficients consisting of the distance between the system state point and the sliding mode surface. A quasi-sliding mode based on hyperbolic tangent saturation function with adjustable boundary layer is utilized to overcome the inertia generated by time delay and space lag.

Different from the CERL, the system state variable x is added as the distance between the system state point and the sliding mode surface. Thereby, as the system state point gradually approaches the sliding mode surface, x decreases, and the reaching speed and chattering decrease accordingly. The specific derivation process is shown as follows.

1) Add a function $f(x)$ among the isokinetic reach term which satisfies

$$\begin{cases} \lim\limits_{x\to 0} f(x) = 0 \\ \forall x \in R,\ f(x) < 1 \text{and} \lim\limits_{x\to\infty} f(x) = 1 \end{cases} \tag{2}$$

such that when the system state trajectory is approaching and finally reaching the sliding mode surface, $f(x)$ gradually decreases and eventually converges to zero. Meanwhile, the variable gain $\eta f(x)$ is always smaller than the original isokinetic gain η independent of the approaching process. Thereby, the sliding mode chatting suppression can be realized effectively without sacrificing the reaching speed.

2) Introduce a power function $|x|^{\beta}$ among the exponential reaching term which satisfies $0<\beta<2$, such that the reaching speed is high at the beginning of the approaching motion, and gradually converges to zero as the system state variable x reaches the sliding mode surface. Thus, the NRL can be adaptive to the changes of system states and sliding mode surface and then improves the dynamic performance.

3) Combine a saturation function $g(s)$ to the symbolic function sgn(s) to reduce the sawtooth trajectory caused by the hysteresis of the switch in time and space, and the inherent inertia of the system, such that the sliding mode chattering can be reduced. The saturation function $g(x)$ must satisfy

$$\begin{cases} g(s) \text{ is odd} \\ \lim\limits_{s\to+\infty} g(s) = 1 \text{ or } \exists s \in R, g(s) = 1 \end{cases}. \tag{3}$$

The hyperbolic tangent function tanh(s) can be a good choice.

4) Mathematically, the function $f(x)$ can be designed as

$$f(x) = \frac{|x|^{\rho}}{|x|^{\rho} + \alpha}, \alpha > 0 \tag{4}$$

where α is a variable term coefficient, and ρ the exponent or the power to be determined.

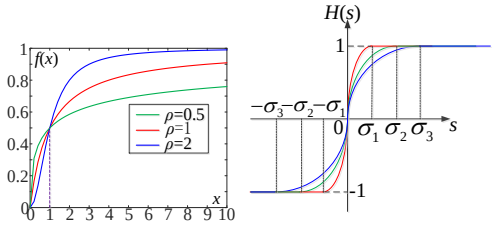

Fig. 1. (a) Function $f(x)$ with different powers. (b) Various boundary layer widths of the hyperbolic tangent function.

Fig. 1 (a) shows the curves of function $f(x)$ with different values of power, where only the positive part is given as the $f(x)$ is an even function. When x=1, no matter what value of ρ, $f(x)$ is a constant and the point x=1 is a turning point. For ρ=2, when x>1, $f(x)$ has a large value, meaning a high reaching speed. However, when x<1, the $f(x)$ decreases rapidly, resulting in a low convergence speed, which is not conducive to quickly eliminate the error. For ρ=0.5, contrary to the situation of ρ=2, $f(x)$ has a low reaching speed when x>1. Thus, it is a tradeoff to select ρ=1.

The piecewise function $H(s)$ comprised of a saturation function $g(x)$ and a symbolic function sgn(s) is defined as

$$H(s) = \begin{cases} \text{sgn}(s) & |s| \ge \sigma \\ \tanh(\mu s) & |s| < \sigma \end{cases} \tag{5}$$

where μ=2π/σ, and σ is the width of the boundary layer. The chattering suppression becomes evident as the width of the boundary layer increases. However, the response speed of the sliding mode soft switching and robustness of the system will decrease. The various boundary layer widths of the hyperbolic tangent function are shown in Fig. 1 (b).

Finally, the NRL is established as

$$\frac{ds}{dt} = -\frac{\eta|x|}{|x|+\alpha} H(s) - k|x|^{\beta} s, \quad \alpha > 0, 0 < \beta < 2 \tag{6}$$

In order to verify the stability of the NRL, the Lyapunov function V=s^2/2 is chosen. The following sliding mode arrival condition will be satisfied if the following formula is met.

$$\dot{V} = s\dot{s} \le 0 \tag{7}$$

Substituting the NRL (6) into (7), one obtains

$$\dot{V} = s\dot{s} = \begin{cases} -\dfrac{\eta|x||s|}{|x|+\alpha} - k|x|^{\beta} s^2 & |s| \ge \sigma \\ -\dfrac{\eta|x| s \tanh(\mu s)}{|x|+\alpha} - k|x|^{\beta} s^2 & |s| < \sigma \end{cases} \tag{8}$$

Since $\dot{V}\le 0$ for both $|s|\ge\sigma$ and $|s|<\sigma$, as shown by (8), the proposed NRL satisfies the sliding mode arrival condition and can ensure that the system motion trajectory reaches the sliding mode switching surface within a limited time.

III. Design of SMSC Based on NRL in DTC System

A. Function and Mathematic Model of Speed Controller

Fig. 2 shows the schematic diagram of the PI speed controller in the speed loop of the conventional DTC system. The PI speed controller module outputs the reference torque according to the torque and speed errors. It is widely used in the speed loop control due to its simple structure. Despite the merit of simplicity, the PI controller behaves modestly in the aspects of anti-disturbance and nonlinear control compared with the SMC. The abilities of anti-disturbance and precise nonlinear control are essential to reduce the torque ripples of the SRM DTC drive system, which is the main purpose of this paper. Replacing the PI controller innovatively, the SMC has strong robustness and can overcome the system uncertainties due to interference and unmodeled dynamics. It is especially suitable for the control of nonlinear systems.

In this section, the design of an SMSC based on the NRL is presented. According to the mechanical movement equation of the motor, the mathematic model of the speed loop in the DTC system can be expressed as

$$\dot{\omega} = \frac{1}{J}(T_e - T_L - D\omega) \tag{9}$$

where J, ω, T_e, T_L and D are the moment of inertia, angular speed, electromagnetic torque, load torque and damping coefficient, respectively.

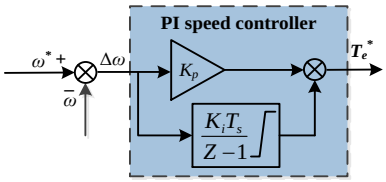

Fig. 2. Schematic diagram of the PI speed controller in the speed loop of the DTC system.

B. Design of SMSC with NRL

The speed controller should be designed such that it can control the actual motor speed ω to accurately track the reference speed ω^* against any internal parameter perturbation and external disturbance. To realize this goal, the speed tracking error defined as

$$e = \omega^* - \omega \tag{10}$$

should be minimized.

The design of an SMSC includes two main steps: design a suitable sliding mode switching surface and control the output of sliding mode control based on the sliding mode reaching law.

The sliding mode switching surface is designed as

$$s = e = \omega^* - \omega \tag{11}$$

Taking derivatives of both sides of (11), one obtains

$$\dot{s} = \dot{\omega}^* - \dot{\omega} \tag{12}$$

Substituting (12) into (9) yields

$$\dot{s} = \dot{\omega}^* - \frac{1}{J}(T_e - T_L - D\omega) \tag{13}$$

Incorporating the NRL into (13), we obtain

$$-\frac{\eta|x|}{|x|+\alpha}H(s)-k|x|^{\beta}s=\dot{\omega}^{*}-\frac{1}{J}(T_e-T_L-D\omega) \tag{14}$$

Finally, the output of SMSC of the SRM based on the NRL, or the reference torque T_e^* of the speed loop of the DTC system can be obtained as

$$T_e^{*}=J\dot{\omega}^{*}+T_L+D\omega+\frac{J\eta|x|}{|x|+\alpha}H(s)+Jk|x|^{\beta}s \tag{15}$$

By tracking this torque reference, the torque of the SRM can be controlled.

Fig. 3 illustrates a schematic diagram of the SMSC. The calculation process of reference torque designed in this section is relatively easy to build in Matlab/Simulink.

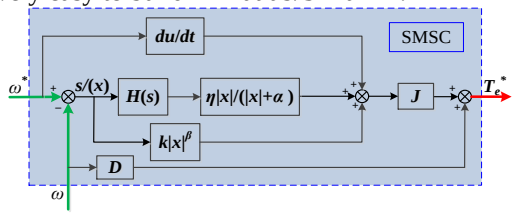

Fig. 3. Schematic diagram of the sliding mode speed controller.

IV. Design of ADSMO and a Composite Speed Control Strategy

According to the above analysis, to improve the accuracy of the DTC system and reduce the torque ripple, the reference torque T_e^* and the observed actual torque T_e play significant roles. A key factor affecting the accuracy of torque estimation is the disturbance caused by mechanical parameters, such as the moment of inertia J, load torque T_L, and damping coefficient D. Thus, in this section, a disturbance estimation method based on SMO is proposed to estimate the real-time disturbance. By feeding the estimated value of disturbance forward to the SMSC above, the anti-disturbance performance of the system can be effectively improved.

A. Mathematic Model of SMO

According to the mechanical movement formula (9), considering the parameter changes and external disturbances, one can express the dynamic motor equation as

$$J_0\dot{\omega}=T_e-D_0\omega+r \tag{16}$$

where J_0 and D_0 are rough estimations of the moment of inertia and damping coefficient, respectively. They satisfy $J=J_0+\Delta J$, $D=D_0+\Delta D$, respectively, where ΔJ and ΔD are parameter errors between the true system and their crude estimations.

In (16), r is the sum of disturbances, including the internal parameter changes and external load disturbances, expressed as

$$r=-\Delta J\dot{\omega}-T_L-\Delta D\omega \tag{17}$$

By taking the disturbance as an extended state variable of the system, the dynamic equation of the motor in the form of state equation can be obtained from (16) as

$$\begin{cases}J_0\dot{\omega}=T_e-D_0\omega+r\\ \dot{r}=d\end{cases} \tag{18}$$

where d is the variation rate of system disturbances r. Therefore, an ADSMO can be constructed as the following:

$$\begin{cases}\dot{\hat{\omega}}=\dfrac{1}{J_0}(T_e-D_0\hat{\omega}+\hat{r}+S_{smo})\\ \dot{\hat{r}}=pS_{smo}\end{cases} \tag{19}$$

where p is the sliding mode parameter, $\hat{\omega}$ is estimated speed, $\hat{r}$ is estimated disturbance, S_{smo} is the switch function of SMO, and

$$S_{smo}=-\lambda\,\mathrm{sgn}(S) \tag{20}$$

where λ is the switching coefficient satisfied where $\lambda>0$, and $S=\hat{\omega}-\omega$ the switching surface satisfied.

By subtracting the ADSMO (19) from the extended state (18), the error equation can be expressed as

$$\begin{cases}J_0\dot{e}_1=-D_0e_1+e_2+S_{smo}\\ \dot{e}_2=pS_{smo}-d\end{cases} \tag{21}$$

where $e_1=S$, and $e_2=\hat{r}-r$.

B. Parameter Selection and Chattering Suppression Analysis

To ensure the occurrence of the sliding mode, it is essential to select proper observer parameters. The sliding mode arrival condition (equivalent to the stability condition) can be utilized to decide the range of the observer parameters. Assume that the sliding mode stability condition is satisfied under the Lyapunov function $V=e_1^2/2$. Substituting (21) into the sliding mode stability equation $e_1\dot{e}_1<0$, one can obtain

$$\begin{aligned}e_1\dot{e}_1&=\frac{1}{J_0}e_1(-D_0e_1+e_2+S_{smo})\\&=\frac{1}{J_0}e_1[(-D_0e_1+e_2)-\lambda\,\mathrm{sgn}(e_1)]\\&=\begin{cases}\dfrac{1}{J_0}e_1[(-D_0e_1+e_2)-\lambda],\ e_1>0\\ \dfrac{1}{J_0}e_1[(-D_0e_1+e_2)+\lambda],\ e_1<0\end{cases}<0\end{aligned} \tag{22}$$

To ensure that (22) is satisfied, the parameter λ must meet

$$\lambda>m|-D_0e_1+e_2| \tag{23}$$

where m ($m>1$) is a safety factor of sliding mode to guarantee the observer's stability. In practical applications, $m=2$ is usually sufficient. Thus, the parameters can be selected by

$$\lambda>2|-D_0e_1+e_2| \tag{24}$$

When the system state arrives and remains on the switching surface, $de_1/dt=e_1=0$. Thus, (21) can be simplified as

$$\begin{cases}e_2=-S_{smo}\\ \dot{e}_2=pS_{smo}-d\end{cases}. \tag{25}$$

This equation can be further written as

$$\dot{e}_2+pe_2+d=0 \tag{26}$$

Solving (26), the disturbance estimation error can be obtained as

$$e_2=e^{-pt}(C+\int d\cdot e^{pt}dt) \tag{27}$$

where C is a constant. To ensure that the disturbance estimation error e_2 converges to zero, the sliding mode parameter is selected as

$$p > 0 \tag{28}$$

Simultaneously, parameter p affects the convergence rate of error e_2 directly.

The above analysis shows that the selection of ADSMO parameters should meet the requirements shown in (24) and (28). Fig.4 illustrates a schematic diagram of ADSMO.

In order to consider the chattering effect on the ADSMO proposed in this paper, the first equation in the error equation (25) is rewritten as the following

$$e_2 = -S_{smo} + Y \tag{29}$$

where Y represents the chattering signal. Substituting (29) into the second formula of (25), one can obtain

$$\dot{e}_2 + pe_2 = pY - d \tag{30}$$

From (30), the transfer function of the observer error e_2 can be obtained as

$$F(s) = \frac{e_2}{Y - d/p} = \frac{1}{s/p + 1} \tag{31}$$

Let T=1/p, and (31) can be expressed as

$$F(s) = \frac{e_2}{Y - Td} = \frac{1}{Ts + 1} \tag{32}$$

The transfer function $F(s)$ in (32) is a low-pass filter with a cutoff frequency of p and is capable of suppressing effectively high-frequency signals. Therefore, the disturbance estimation $\hat{r}$ can be directly applied to the control system without the need of an additional low-pass filter to suppress chattering. The chattering suppression effect can be adjusted by varying the cutoff frequency p to meet the control system requirements.

C. Composite Speed Control Strategy Based on ADSMO

In order to improve the anti-disturbance ability of the DTC system, an anti-disturbance speed control strategy is developed based on the ADSMO and the new sliding mode speed controller. Fig. 5 shows a control block diagram.

The speed loop adopts the SMC based on the NRL, and combines with the ADSMO to update the disturbance in real-time to form a composite speed control strategy of SMSC-ADSMO. The disturbance observed by ADSMO in real-time is fed forward to SMSC for compensating the system's disturbance, and thereby improving the system anti-disturbance capability.

According to the SMSC design in Section III and the dynamic motor equation (16), one can obtain

$$\dot{s} = \dot{\hat{\omega}} - \frac{1}{J_0}(T_e - D_0\omega + r) \tag{33}$$

Substituting the reaching law (6) into (33) yields

$$\begin{aligned} \dot{s} &= \dot{\hat{\omega}} - \frac{1}{J_0}(T_e - D_0\omega + r) \\ &= -\frac{\eta|x|}{|x| + \alpha} H(x) - k|x|^{\beta} s, \quad \alpha > 0, 0 < \beta < 2 \end{aligned} \tag{34}$$

Solving (34), one can obtain

$$T_e^* = J_0 \dot{\hat{\omega}} - r + D_0\omega + \frac{J_0\eta|x|}{|x| + \alpha} H(s) + J_0 k|x|^{\beta} s \tag{35}$$

Fig. 6 illustrates a schematic diagram of the composite speed controller, which consists of an SMSC based on the NRL (Part I), and a system disturbance estimation and compensation loop (Part II). During the actual operation, the control method utilizes the observer to estimate the system disturbance on-line, and feeds the estimated disturbance to the SMSC so as to suppress the influence of various disturbances on the system control performance.

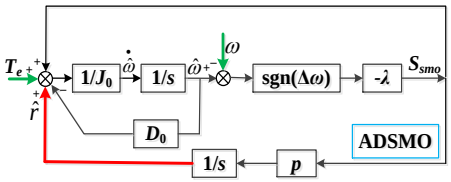

Fig. 4. Schematic diagram of ADSMO.

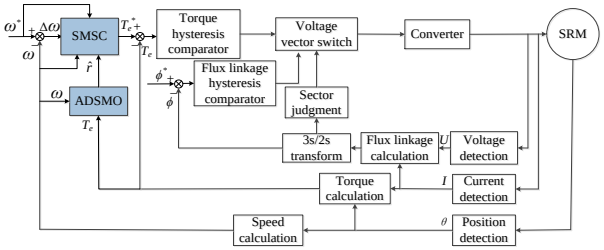

Fig. 5. Control block diagram of the DTC with anti-disturbance speed control.

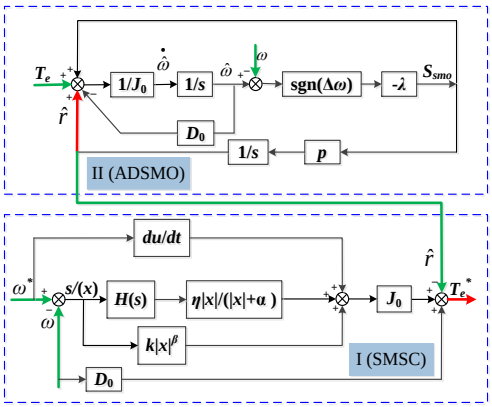

Fig. 6. Schematic diagram of the composite speed controller.

D. Principle of Torque Ripple Reduction of the Proposed Control Scheme

According to the principle of the DTC, it uses torque as the control target directly. Then, compare the measured torque with the expected torque, and combine the torque, the results of the flux linkage hysteresis comparator, and the parameter selection of the switch table to determine the on-off state of the next winding. As shown in the above analysis, the given reference torque T_e^* is obtained by the speed controller. According to the mechanical movement (9), the relationship between the speed and torque is acquired. Assume that the system is in equilibrium at a fixed speed ω, and at this time, $\dot{\omega}$=0 . Thus, (9) can be simplified as

$$T_e = T_L + D\omega \tag{36}$$

The variation of electromagnetic torque T_e will affect the rate of change of speed ω by

$$\Delta T_e = J\dot{\omega} \tag{37}$$

If the time interval Δt is small, it can be deemed that the load torque T_L and damping term $\Delta\omega$ are constant within Δt, i.e.

$$\begin{cases} \dot{\omega} \cong \Delta\omega/\Delta t \\ \Delta T_e = J\Delta\omega/\Delta t \end{cases} \tag{38}$$

Let $K \cong J/\Delta t$, (38) can be written as

$$\Delta T_e = K\Delta\omega \tag{39}$$

According to (39), it can be deduced that the change in electromagnetic torque T_e is proportional to the change in angular velocity ω. Therefore, the torque ripple can be reduced by effective control of the speed deviation.

Since the DTC drive system of SRM is a highly nonlinear control object, the conventional PI speed controller usually fails to be competent for eliminating speed static error, while SMC is adept in nonlinear control. Therefore, the proposed speed controllers based on SMC and SMO is used to control the speed deviation and eliminate speed static error effectively. Besides, SMC regards torque ripple as a disturbance, without knowing the exact model of SRM. Hence, it can effectively suppress torque ripple and greatly improve system performance. The detailed mathematical principles for the SMSC and SMSC-ADSMO composite speed control strategy have been established in (15) and (35), respectively. Their schematic block diagrams are shown in Figs. 3 and 6, respectively. For the PI speed controller, the mathematical principle can be expressed as follows.

$$T_e(z) = K_p\Delta\omega(z) + K_i\sum_{j=0}^{z}\Delta\omega(z) \tag{40}$$

where z represents the z-th sampling moment. The schematic block diagram is shown in Fig. 2.

V. Simulation Validation

To verify the accuracy and effectiveness of the proposed SMSC and ADSMO, simulations are conducted on the DTC system. According to the block diagrams of the PI controller and DTC system shown in Figs. 2 and 5, the DTC system of SRM drive is simulated in Matlab/Simulink. Table I lists the specific parameters of the simulation model and essential SRM parameters [31]. The reference speed is set as 1000 rpm since the DTC is more suitable for low and medium speed range. The switching frequency will be much higher in the high-speed range, which may cause unsteady and large torque ripple according to the DTC principle.

A. Selection of Sliding Mode Parameters

According to Section II, the sliding mode parameters that need to be selected are the isokinetic and exponential reaching coefficients η and k, and the parameters α, β, and σ in the NRL. Among them, η and k are the most sensitive parameters in the SMSC simulation. They must satisfy the reference torque T_e^* outputted by SMSC, with around 15 Nm as the initial state and 0 Nm in the steady state. Thus, we obtain the following restrictions:

$$\begin{cases} J\eta + Jk|x|^{\beta}\, s \approx 15 \quad (s=x \approx \omega^*) \\ D\omega + \dfrac{J\eta|x|}{|x|+\alpha}\tanh(2\pi s/\sigma) + Jk|x|^{\beta}\, s \approx 0 \quad (s=x \approx 0) \end{cases} \tag{41}$$

Set the parameters α, β, and σ as constants firstly, and then limit the range of η and k according to the restrictions. Thereby, they can be adjusted within a small range.

For a very large coefficient η, while the response speed is increased, the chattering also increases apparently. If it is too small, the chattering can be reduced, but the response speed will be slow. The adjustment process of parameter η is shown in Fig. 7. For a very large coefficient k, the initial torque will be large and unstable. If it is too small, the response speed becomes slow. The adjustment process of k is shown in Fig. 8. After the determination of parameters η and k, parameters α, β, and σ are selected for the optimal response speed and chattering suppression.

Finally, the isokinetic and exponential reaching coefficients η and k are set as 12 and 48, respectively. The parameters α, β, and σ in the NRL are set as 1.4, 1.2 and 0.3, respectively. For the PI speed controller, the proportional parameter P is 0.015, and the integral parameter I is 0.01.

TABLE I
Specific Simulation Parameters and Essential Motor Parameters

Parameter	SRM
Number of phases	4
Numbers of stator/rotor poles	16/10
Rated power (kW)	1.8
Rated efficiency	0.85
Reference speed (r/min)	1000
Rated voltage (V)	120
Resistance per phase (Ω)	0.46
Rough moment of inertia J_0 (kg·m^2)	0.0047
Rough damping coefficient D_0 (N·m·s)	0.001
Given flux linkage ϕ^* (Wb)	0.1
Torque hysteresis width (Nm)	0.1
Flux linkage hysteresis width (Wb)	0.01

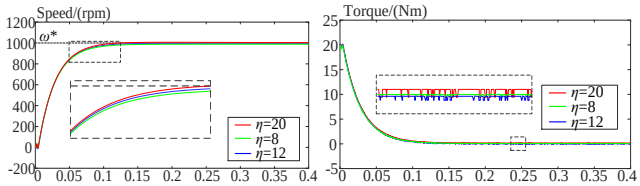

(a) (b)

Fig. 7. Parameter η simulation debugging process. (a) Speed, and (b) Torque.

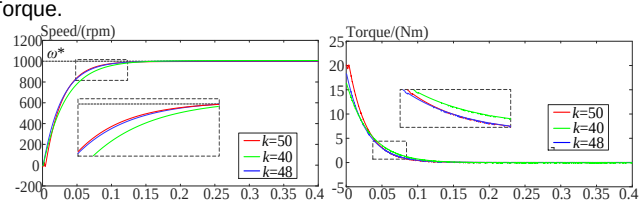

(a) (b)

Fig. 8. Parameter k simulation debugging process. (a) Speed, and (b) Torque.

B. Validation of Proposed NRL and SMSC

Firstly, a comparison of the NRL and CERL in terms of the reaching time is presented according to mathematical analysis. The reaching time of CERL can be calculated by integrating (1) from 0 to t, with $s(t)$=0.

$$t_c = \frac{1}{k}\ln\left(\frac{ks(0)}{\eta}+1\right) \tag{41}$$

where t_c is the reaching time of CERL. Similarly, the reaching time of NRL t_n can be calculated when $|s|\geq\sigma$, as follows.

$$\begin{aligned} t_n &= \frac{1}{k|x|^{\beta}}\ln\left(\frac{ks(0)}{\eta}\left(|x|^{\beta}+\alpha|x|^{\beta-1}\right)+1\right) \\ &< \frac{1}{k|x|^{\beta}}\ln\left(\frac{ks(0)}{\eta}|x|^{\beta}\right) \end{aligned} \tag{42}$$

By comparison, it can be found that

$$t_n - t_c < \frac{1}{k|x|^{\beta}} \ln\left(\frac{ks(0)}{\eta}|x|^{\beta}\right) - \frac{1}{k|x|^{\beta}} \ln\left(\frac{ks(0)}{\eta} + 1\right)^{|x|^{\beta}} < 0 \quad (43)$$

where $|x|>0$ in approaching movement. When $|s|<\sigma$, the same conclusion can be obtained, meaning that the reaching time of NRL is less than that of CERL. It can be verified by the simulation results of phase trajectory of the two reachings, as shown in Fig. 9 (a). Besides, according to the results of error convergence rate, as shown in Fig. 9 (b), it can be found that the NRL improves the convergence speed and reduces the error.

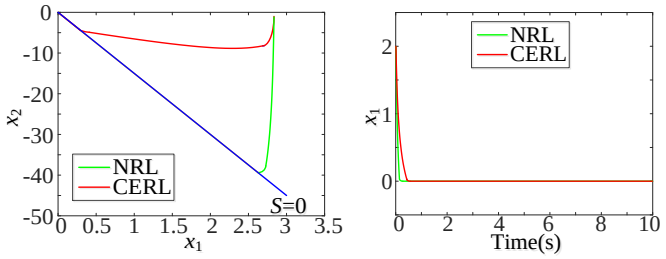

(a) (b)

Fig. 9. Simulation results of the two reaching laws. (a) Phase trajectory, and (b) Error convergence rate.

Secondly, to demonstrate the effectiveness of proposed SMSC, the DTC system with the PI, SMSC with reaching law in [23] (SMSC_23) and proposed SMSC are carried out.

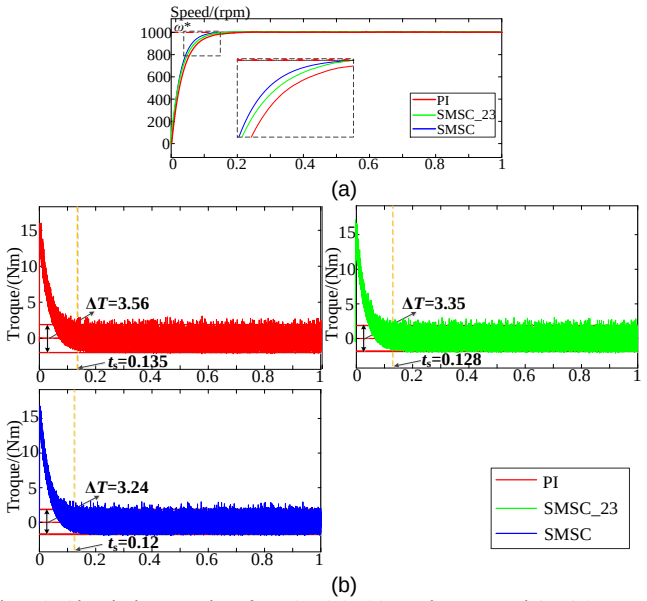

(a)

(b)

Fig. 10. Simulation results of PI, SMSC_23, and proposed SMSC speed control strategies. (a) Speed, and (b) Torque.

Fig. 10 shows the simulation results. As shown, the application of SMSC can improve the dynamic performance and reduce the torque ripples, and the SMSC with the proposed reaching law presents more significant improvements than the SMSC with reaching law in [23], demonstrating the effectiveness of SMSC and the proposed NRL.

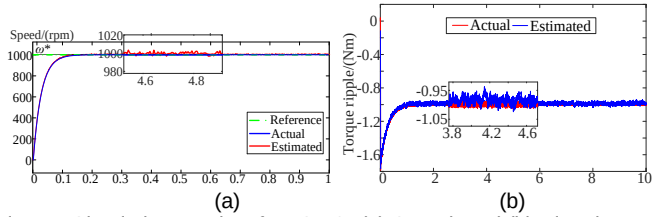

(a) (b)

Fig. 11. Simulation results of ADSMO. (a) Speed, and (b) Disturbance.

C. Validation of ADSMO

To demonstrate the effectiveness of ADSMO, the speed ω and disturbance r estimated by the ADSMO will be obtained by simulating the DTC system with the proposed SMSC-ADSMO composite speed control strategy. During the simulation, the sliding mode parameter p is set as 2 and switch coefficient λ is calculated by (24) in real time.

The simulation results are compared with the actual results, as shown in Fig. 11. As shown, the estimated speed shows good agreement with the actual speed with the error of estimation within 5 r/min. For the disturbance r, according to (20), the disturbance is large at the beginning and then decreases as the speed tends to be stable. The estimated disturbance shows good agreement with the actual disturbance with the error of estimation within 0.1 Nm. Thus, the proposed ADSMO behaves well in estimating real-time disturbance, and the estimated value is fed forward to the SMSC above, so as to improve the anti-disturbance performance of the system.

D. Validation of SMSC-ADSMO

Firstly, demonstrate the principle of torque ripple reduction of the proposed control scheme. The simulation results of reference torque T_e^* outputted by the SMSC-ADSMO and actual torque T_e are illustrated in Fig. 12. As shown, the reference torque can well track the actual torque in real time, so as to reduce the torque error. It is significant for controlling the speed loop of the DTC system, and then reducing the torque ripple. Fig. 13 shows the simulated current of PI and SMSC-ADSMO controllers. As shown, the proposed controller has a smoother current waveform and larger starting current. This is consistent with fast response speed and small torque ripple.

These results reveal that the proposed control schemes are indeed effective in reducing the torque ripples at a given speed. Moreover, the nonlinear control of a nonlinear motor such as SSRM should be clear from the practical point of view. Thus, the torque ripple and torque per ampere over a wide speed range need to be considered to investigate whether or not the proposed control schemes have practical meaning.

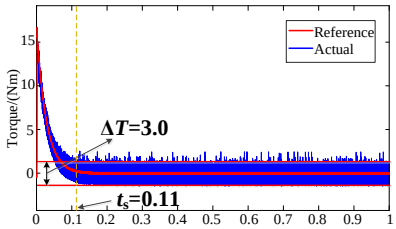

Fig. 12. Simulation results of reference torque outputted by SMSC-ADSMO and actual torque.

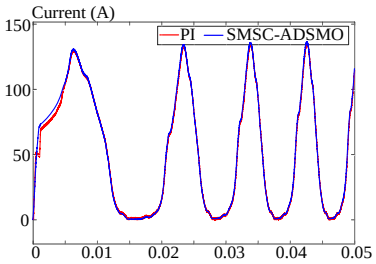

Fig. 13. Simulation results of currents.

Firstly, the torque ripple and torque-ampere ratio are calculated by

$$\delta = T_{\max} - T_{\min} = \Delta T \tag{44}$$

$$\xi = \frac{T_{av}}{i_{av}} \tag{45}$$

where δ, $T_{\max}$, $T_{\min}$, ξ, T_{av} and i_{av} are the torque ripple, maximum torque, minimum torque, torque-ampere ratio, average torque, and average current, respectively. In this paper, T_{av} and i_{av} are calculated by using the simulation results. Reference speed n is selected from 200 to 2000 rpm successively with an interval of 200 rpm. Figs. 14(a) and (b) plot the curves of torque ripple and torque-ampere ratio versus rotating speed under different control schemes, respectively. As shown, the proposed control schemes yield excellent torque ripple reduction and torque-ampere radio in comparison to the conventional PI speed controller.

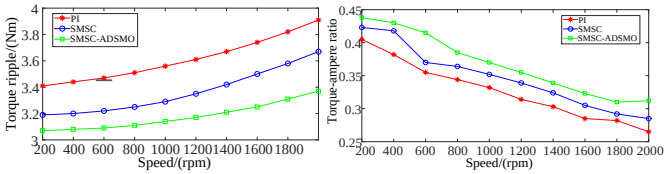

(a) (b)

Fig. 14. Torque ripple and torque-ampere ratio versus different rotating speeds under different control schemes: (a) Torque ripple, and (b) Torque-ampere ratio

VI. Experimental Validation

The effectiveness of the SMSC, proposed NRL and ADSMO have been validated by simulation. In order to further verify the superiority of SMSC-ADSMO composite speed control strategy, the comparisons between it and the PI speed controller are conducted in the experiment. The compared results mainly include startup speed and torque, speed and torque with various loads, and speed and torque with load disturbance.

Fig. 15 shows the test platform, where the 16/10 poles SRM prototype, JN338 torque and speed sensor with 20 Nm torque range, and FZ25J magnetic powder brake with 25 Nm torque range are connected by two couplings. The position is detected by using the Hall sensor ATS675LSE, and then the signal is sent to the dSPACE. Similarly, the current signal captured by the current sensor is sent to the dSPACE for further control. The sampling time is set as 1 ms. Other hardware includes a DC power supply, an asymmetrical half-bridge circuit, a PC and an oscilloscope. Fig. 16 shows a block diagram of the experimental setup. The control strategy in the dSPACE controller board is compiled from the Matlab/Simulink script by a real-time code generation and download software. The specific experimental parameters are the same as the simulation parameters as listed in Table I.

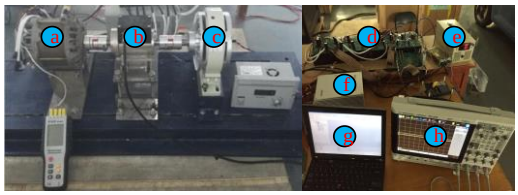

Fig. 15. Devices and platform for testing dynamic characteristics: (a) 16/10 pole SRM, (b) Torque and speed sensor, (c) Magnetic powder brake, (d) Power converter and drive circuit, (e) Power supply, (f) dSPACE, (g) PC, and (h) Oscilloscope.

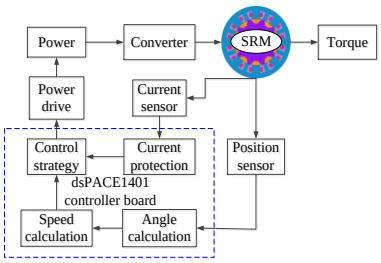

Fig. 16. Block diagram of the experimental setup.

During the experiment, the DTC systems based on various control strategies are programmed in the dSPACE control system, respectively. In order to make a fair and intuitive comparison, the same sampling method and speed are applied to all control strategies, and the voltage level is also kept the same as that the division indicates. Figs. 17 and 18 illustrate the experimental results recorded by the oscilloscope.

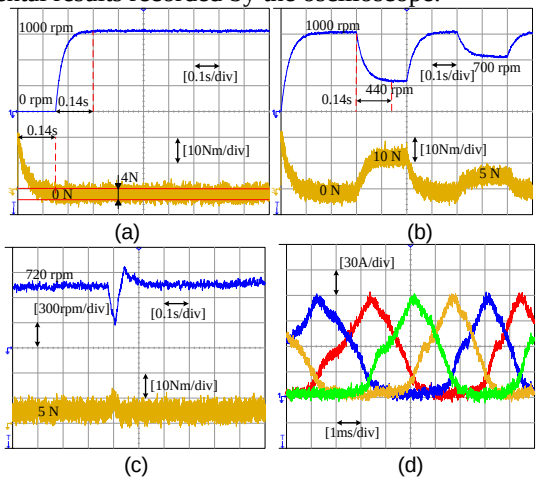

Fig. 17. Experimental results with PI speed controller. (a) Startup speed and torque, (b) Speed and torque with various loads, (c) Speed and torque with load disturbance, and (d) Current at 1000 rpm.

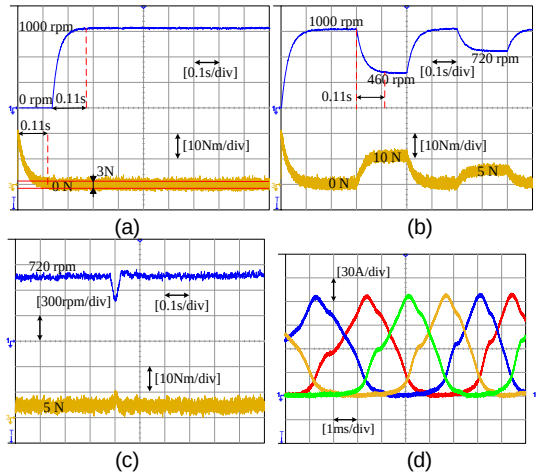

Fig. 18. Experimental results with SMSC-ADSMO composite speed control strategy. (a) Starting speed and torque, (b) Speed and torque with various loads, (c) Speed and torque with load disturbance, and (d) Current at 1000 rpm.

As shown by the speed curves, the response times of the two control strategies are 0.14 and 0.11 s, respectively. The torque curves show that the torque response times of the two control strategies are 0.14 and 0.11 s, respectively, which are consistent with the speed response times. The torque ripple ranges are approximately 4 and 3 Nm, respectively. The current

waveforms of the proposed method behave more stable and smoother than the PI method. It can be concluded that the proposed SMSC-ADSMO composite speed control strategy can perform well to improve the response time and torque ripple suppression.

To further verify the effectiveness of the ADSMO, parameter mismatch experimental results are presented in Fig. 19. Set the mechanical parameters moment of inertia J and damping coefficient D respectively to observe the disturbance r under the circumstances of parameter mismatch. As shown, The change of moment of inertia affects the initial disturbance, the change of damping coefficient affects the stable disturbance, and the estimated disturbance can follow the actual disturbance well no matter how the parameter mismatch is.

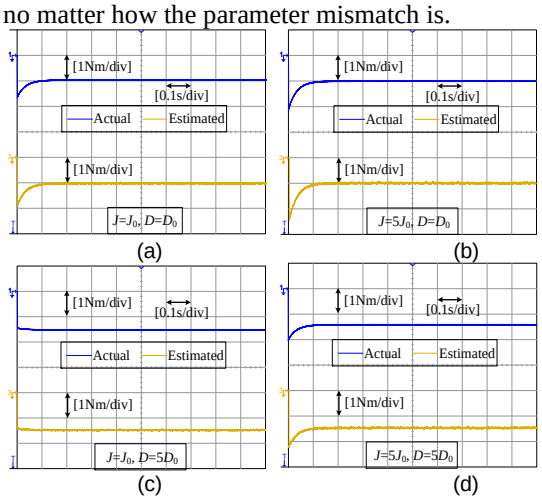

Fig. 19. Parameters mismatch experimental results of disturbance: (a) J=J_0, D=D_0, (b) J=5J_0, D=D_0, (c) J=J_0, D=5D_0, and (b) J=5J_0, D=5D_0.

The speed and torque curves under various loads show that the dynamic response time between two different loads of the two control strategies are 0.14 and 0.11 s, respectively. The speed and torque curves in the presence of load disturbance show that, as the same load disturbance occurs, the SMSC-ADSMO composite speed control strategy can perform better because of its unique ADSMO module, which is via estimating and feeding the system disturbance on-line during the actual operation to reduce the influence of various disturbances and realize the disturbance self-suppression control.

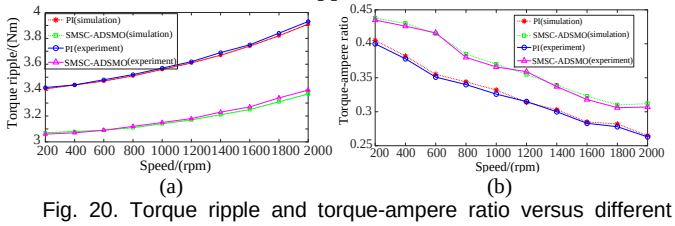

Fig. 20. Torque ripple and torque-ampere ratio versus different rotation speeds under the two control schemes: (a) Torque ripple, and (b) Torque-ampere ratio.

The superiority of SMSC-ADSMO composite speed control strategy on response time, torque ripple reduction, and disturbance suppression has been validated for the SRM drive. Table II lists a quantitative analysis of some significant performance results of PI controller and SMSC-ADSMO under different speeds and loads. Fig. 20 illustrates the torque ripple and torque-ampere ratio curves of the two control schemes in terms of different speeds. As shown, there is a good agreement between the simulation and experimental results, which validates the practical effectiveness of the proposed SMSC-ADSMO.

TABLE II
PERFORMANCE RESULTS OF TWO CONTROL STRATEGIES

		PI	SMSC-ADSMO
Speed response time (s) (different speeds)	1000 rpm	0.14	0.11
	700 rpm	0.12	0.10
	440 rpm	0.14	0.11
Torque response time (s) (different loads)	0 N	0.14	0.11
	5 N	0.12	0.10
	10 N	0.14	0.11
Torque ripple range (Nm) (different loads)	0 N	4.0	3.0
	5 N	3.8	2.8
	10 N	3.6	2.6

VII. CONCLUSION

In this paper, an improved DTC with SMC and SMO was proposed to reduce the torque ripple of the SRM drive system. The following conclusions can be drawn through the theoretical analysis and discussions of the simulation and experimental results.

(1) By utilizing the new reaching law, the dilemma to increase the reaching speed and reduce the sliding chattering can be solved.

(2) By reducing the speed deviation, the proposed SMSC shortens the response time, and reduces the torque ripple of the conventional DTC.

(3) The ADSMO is effective in improving the anti-disturbance ability of the DTC system. Thus, the composite control strategy SMSC-ADSMO can further reduce the torque ripple.

(4) As demonstrated by the simulation and validated by the experimental test, the proposed SMSC-ADSMO composite speed control strategy performs well in torque ripple reduction since it can effectively control the speed deviation. Besides, response speed, anti-disturbance ability, and torque-ampere ratio are also improved.

REFERENCES

[1] C. Ho, J. Wang, H. Hu, and C. Liaw, "Development and operation control of a switched-reluctance motor driven flywheel," *IEEE Trans. Power Electron.*, vol. 34, no. 1, pp. 526-537, Jan. 2019.

[2] X. Sun, C. Hu, G. Lei, Y. Guo, and J. Zhu, "State feedback control for a PM hub motor based on grey wolf optimization algorithm," *IEEE Trans. Power Electron.*, vol. 35, no. 1, pp. 1136-1146, Jan. 2020.

[3] X. Sun, K. Diao, G. Lei, Y. Guo, and J. Zhu, "Real-time HIL emulation for a segmented-rotor switched reluctance motor using a new magnetic equivalent circuit," *IEEE Trans. Power Electron.*, vol. 35, no. 4, pp. 3841-3849, Apr. 2020.

[4] X. Sun, J. Cao, G. Lei, Y. Guo, and J. Zhu, "Speed sensorless control for permanent magnet synchronous motors based on finite position set," *IEEE Trans. Ind. Electron.*, vol. 67, no. 7, pp. 6089-6100, Jul. 2020.

[5] H. Li, B. Bilgin, and A. Emadi, "An improved torque sharing function for torque ripple reduction in switched reluctance machines," *IEEE Trans. Power Electron.*, vol. 34, no. 2, pp. 1635-1644, Feb. 2019.

[6] L. Liu, M. Zhao, X. Yuan, and Y. Ruan, "Direct instantaneous torque control system for switched reluctance motor in electric vehicles," *The Journal of Engineering*, vol. 2019, no. 16, pp. 1847-1852, 2019.

[7] G. H. B. Foo and X. Zhang, "Robust constant switching frequency-based field-weakening algorithm for direct torque controlled reluctance synchronous motors," *IEEE Trans. Ind. Inform.*, vol. 12, no. 4, pp. 1462-1473, 2016.

[8] Y. Sozer, I. Husain, and D. A Torrey, "Guidance in selecting advanced control techniques for switched reluctance machine drives in emerging applications," *IEEE Trans. Ind. Appl.*, vol. 51, no. 6, pp. 4505-4514, Nov./Dec. 2015.

[9] P. K. Reddy, D. Ronanki, and P. Perumal, "Efficiency improvement and torque ripple minimization of four-phase switched reluctance motor drive using new direct torque control strategy," *IET Electric Power Appl.*, vol. 14, no. 1, pp. 52-61, 2020.
[10] S. K Sahoo, S. Dasgupta, S. K Panda, and J. Xu, "A Lyapunov function-based robust direct torque controller for a switched reluctance motor drive system," *IEEE Trans. Power Electron.*, vol. 27, no. 2, pp. 555-564, Feb. 2012.
[11] T. Husain, A. Elrayyah, Y. Sozer, and I. Husain, "Unified control for switched reluctance motors for wide speed operation," *IEEE Trans. Ind. Electron.*, vol. 66, no. 5, pp. 3401-3411, May 2019.
[12] N. Yan, X. Cao, and Z. Deng, "Direct torque control for switched reluctance motor to obtain high torque-ampere ratio," *IEEE Trans. Ind. Electron.*, vol. 66, no. 7, pp. 5144-5152, Jul. 2019.
[13] D. T. Tran, D. X. Ba, and K. K. Ahn, "Adaptive backstepping sliding mode control for equilibrium position tracking of an electrohydraulic elastic manipulator," *IEEE Trans. Ind. Electron.*, vol. 67, no. 5, pp. 3860-3869, 2020.
[14] W. Qi, G. Zong, and H. R. Karimi, "Sliding mode control for nonlinear stochastic semi-markov switching systems with application to SRMM," *IEEE Trans. Ind. Electron.*, vol. 67, no. 5, pp. 3955-3966, 2020.
[15] H. Hou, X. Yu, L. Xu, K. Rsetam, and Z. Cao, "Finite-Time continuous terminal sliding mode control of servo motor systems," *IEEE Trans. Ind. Electron.*, vol. 67, no. 7, pp. 5647-5656, 2020.
[16] H. Ríos, R. Falcón, O. A. González, and A. Dzul, "Continuous sliding-mode control strategies for quadrotor robust tracking: real-time application," *IEEE Trans. Ind. Electron.*, vol. 66, no. 2, pp. 1264-1272, 2019.
[17] D. T. Tran, D. X. Ba, and K. K. Ahn, "Adaptive backstepping sliding mode control for equilibrium position tracking of an electrohydraulic elastic manipulator," *IEEE Trans. Ind. Electron.*, vol. 67, no. 5, pp. 3860-3869, 2020.
[18] K. Shao, J. Zheng, K. Huang, H. Wang, Z. Man, and M. Fu, "Finite-time control of a linear motor positioner using adaptive recursive terminal sliding mode," *IEEE Trans. Ind. Electron.*, vol. 67, no. 8, pp. 6659-6668, 2020.
[19] J. Ye, P. Malysz, and A. Emadi, "A fixed-switching-frequency integral sliding mode current controller for switched reluctance motor drives," *IEEE J. Emerg. Sel. Topics Power Electron*., vol. 3, no. 2, pp. 381-394, Jun. 2015.
[20] W. Shang, S. Zhao, Y. Shen, and Z., Qi, "A sliding mode flux-linkage controller with integral compensation for switched reluctance motor," *IEEE Trans. Mag.*, vol. 45, no. 9, pp. 3322-3328, Sep. 2009.
[21] P. Brandstetter and P. Krna, "Sensorless control of switched reluctance motor using sliding mode observer," *in Proc. 2013 International Conference on Applied Electronics*, pp. 1-4, 2013.
[22] Y. Saadi, R. Sehab, A. Chaibet, M. Boukhnifer, and D. Diallo, "Sensorless control of switched reluctance motor with unknown load torque for EV application using Extended Kalman filter and second order sliding mode observer," *in Proc. 2018 IEEE International Conference on Industrial Technology (ICIT)*, pp. 522-528, 2018.
[23] S. Lin, Y. Cai, B. Yang, and W. Zhang, "Electrical line-shafting control for motor speed synchronization using sliding mode controller and disturbance observer," *IET Control Theory & Applications*, vol. 11, no. 2, pp. 205-212, 2017.
[24] H. Ma and Y. Li, "A novel dead zone reaching law of discrete-time sliding mode control with disturbance compensation," *IEEE Trans. Ind. Electron.*, vol. 67, no. 6, pp. 4815-4825, 2020.
[25] A. Bartoszewicz and P. Leśniewski, "New switching and nonswitching type reaching laws for SMC of discrete time systems," *IEEE Trans. Control Syst. Technol.*, vol. 24, no. 2, pp. 670-677, Mar. 2016.
[26] X. Zhang and Z. Li, "Sliding-mode observer-based mechanical parameter estimation for permanent magnet synchronous motor," *IEEE Trans. Power Electron.*, vol. 31, no. 8, pp. 5732-5745, Aug. 2016.
[27] M. Comanescu, "Design and implementation of a highly robust sensorless sliding mode observer for the flux magnitude of the induction motor," *IEEE Trans. Energy Convers.*, vol. 31, no. 2, pp. 649-657, Jun. 2016.
[28] X. Zhang, L. Sun, K. Zhao, and L. Sun, "Nonlinear speed control for PMSM system using sliding-mode control and disturbance compensation techniques," *IEEE Trans. Power Electron.*, vol. 28, no. 3, pp. 1358-1365, Mar. 2013.
[29] Y. Zhang, Z. Yin, Y. Zhang, J. Liu, and X. Tong, "A novel sliding mode observer with optimized constant rate reaching law for sensorless control of induction motor," *IEEE Trans. Ind. Electron.*, vol. 67, no. 7, pp. 5867-5878, 2020.
[30] C. Gong, Y. Hu, J. Gao, Y. Wang, and L. Yan, "An improved delay-suppressed sliding-mode observer for sensorless vector-controlled PMSM," *IEEE Trans. Ind. Electron.*, vol. 67, no. 7, pp. 5913-5923, 2020.
[31] X. Sun, K. Diao, G. Lei, L. Chen, Y. Guo, and J. Zhu, "Study on segmented-rotor switched reluctance motors with different rotor pole numbers for BSG system of hybrid electric vehicles," *IEEE Trans. Veh. Technol.*, vol. 68, no. 6, pp. 5537-5547, Jun. 2019.

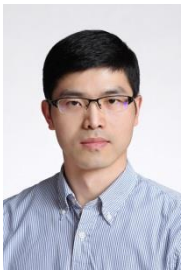

Xiaodong Sun (M'12-SM'18) received the B.Sc. degree in electrical engineering, and the M.Sc. and Ph.D. degrees in control engineering from Jiangsu University, Zhenjiang, China, in 2004, 2008, and 2011, respectively.

Since 2004, he has been with Jiangsu University, where he is currently a Professor in Vehicle Engineering with the Automotive Engineering Research Institute. From 2014 to 2015, he was a Visiting Professor with the School of Electrical, Mechanical, and Mechatronic Systems, University of Technology Sydney, Sydney, Australia. His current teaching and research interests include electrical machines and drives, drives and control for electric vehicles, and intelligent control. He is the author or coauthor of more than 100 refereed technical papers and one book, and he is the holder of 42 patents in his areas of interest. Dr. Sun is an Editor of the IEEE TRANSACTIONS ON ENERGY CONVERSION.

Jiangling Wu received the B.Eng. degree in Vehicle engineering from Jiangsu University, Zhenjiang, China, in 2018, and is currently working toward the M. Eng. degree at Jiangsu University, Zhenjiang, China.

His current research interests include modeling, structure designing and controlling of switched reluctance motors for electric vehicle propulsion.

Gang Lei (M'14) received the B.S. degree in Mathematics from Huanggang Normal University, China, in 2003, the M.S. degree in Mathematics and Ph.D. degree in Electrical Engineering from Huazhong University of Science and Technology, China, in 2006 and 2009, respectively.

He is currently a Senior Lecturer at the School of Electrical and Data Engineering, University of Technology Sydney (UTS), Australia. His research interests include computational electromagnetics, design optimization and control of electrical drive systems and renewable energy systems. He is an Associate Editor of the IEEE TRANSACTIONS ON INDUSTRIAL ELECTRONICS.

Youguang Guo (S'02-M'05-SM'06) received the B.E. degree from Huazhong University of Science and Technology, China in 1985, the M.E. degree from Zhejiang University, China in 1988, and the Ph.D. degree from University of Technology, Sydney (UTS), Australia in 2004, all in electrical engineering. He is currently a Professor in Electrical Engineering at the School of Electrical and Data Engineering, University of Technology Sydney (UTS). His research fields include measurement and modeling of properties of magnetic materials, numerical analysis of electromagnetic field, electrical machine design optimization, power electronic drives and control.

Jianguo Zhu (S'93–M'96–SM'03) received the B.E. degree in 1982 from Jiangsu Institute of Technology, Jiangsu, China, the M.E. degree in 1987 from Shanghai University of Technology, Shanghai, China, and the Ph.D. degree in 1995 from the University of Technology Sydney (UTS), Sydney, Australia, all in electrical engineering. He was appointed a lecturer at UTS in 1994 and promoted to full professor in 2004 and Distinguished Professor of Electrical Engineering in 2017. At UTS, he has held various leadership positions, including the Head of School for School of Electrical, Mechanical and Mechatronic Systems and Director for Centre of Electrical Machines and Power Electronics. In 2018, he joined the University of Sydney, Australia, as a full professor and Head of School for School of Electrical and Information Engineering. His research interests include computational electromagnetics, measurement and modelling of magnetic properties of materials, electrical machines and drives, power electronics, renewable energy systems and smart micro grids.